

Review

Recent In Situ/Operando Spectroscopy Studies of Heterogeneous Catalysis with Reducible Metal Oxides as Supports

Fei Wang¹, Jianzhun Jiang^{2,*} and Bin Wang^{2,*}

¹ State Key Laboratory of Coal Conversion, Institute of Coal Chemistry, Chinese Academy of Sciences, Taiyuan 030001, China; wangfei908@sxicc.ac.cn

² Beijing Research Institute of Chemical Industry, Sinopec Group, Beijing 100013, China

* Correspondence: jiangjz.bjhy@sinopec.com (J.J.); wangbin.bjhy@sinopec.com (B.W.)

Received: 28 April 2019; Accepted: 21 May 2019; Published: 23 May 2019



Abstract: For heterogeneous catalysis, the metal catalysts supported on reducible metal oxides, especially CeO₂ and TiO₂, have long been a research focus because of their excellent catalytic performance in a variety of catalytic reactions. Detailed understanding of the promotion effect of reducible metal oxides on catalytic reactions is beneficial to the rational design of new catalysts. The important catalytic roles of reducible metal oxides are attributed to their intimate interactions with the supported metals (e.g., strong metal-support interaction, electronic metal-support interaction) and unique support structures (e.g., oxygen vacancy, reversible valence change, surface hydroxyl). However, the structures of the catalysts and reaction mechanisms are strongly affected by environmental conditions. For this reason, in situ/operando spectroscopy studies under working conditions are necessary to obtain accurate information about the structure-activity relationship. In this review, the recent applications of the in situ/operando spectroscopy methodology on metal catalysts with reducible metal oxides as supports are summarized.

Keywords: metal catalysts; reducible metal oxides; in situ/operando spectroscopy methodology

1. Introduction

The development of spectral characterization techniques has had a significant impact on catalysis science in revealing the structure-activity relationship [1,2]. By virtue of spectroscopy methodology (e.g., XRD, XAFS, IR, Raman, XPS), the geometrical and electronic structures of the catalytic active site and reaction intermediates can be well characterized. However, they are strongly affected by environmental conditions (atmosphere, temperature, pressure, etc.) [3]. Based on the characterization results in ex situ conditions, an incorrect structure-activity relationship will probably be obtained. It is therefore important to accurately simulate the realistic operation conditions by applying appropriate in situ cells in spectroscopy studies. With the development of in situ/operando spectroscopy methodology, it provides an effective way to identify the intrinsic active sites and corresponding reaction intermediates in real catalytic reactions [4,5].

Reducible oxides (e.g., TiO₂, CeO₂) supported metal catalysts have attracted extensive attention, due to their excellent catalytic performance in many important reactions (e.g., CO oxidation [6–9], water–gas shift reaction [10–13], CO₂ hydrogenation reactions [14–18]). The reducible oxides are supposed to play roles via several routes, including intimate metal-support interactions (e.g., oxides encapsulation of metal nanoparticles [19], electronic interactions [20], metal nanoparticle stabilization [21]) and high-performance metal-support interfacial active sites (e.g., support participation in catalysis [22]). In order to distinguish which of them is the most important, great efforts have been devoted to obtaining

structural information of active sites and reaction mechanisms by applying situ/operando spectroscopy methodology under practical conditions.

In the present work, apart from addressing the key scientific problems encountered by heterogeneous catalysis with reducible oxides as supports, the emphasis is on recent contributions of in situ/operando spectroscopy studies that try to address these problems. We propose current challenges and future strategies for further development of in situ/operando spectroscopy studies in this area.

2. Intimate Metal-Support Interaction

2.1. Strong Metal-Support Interaction

The strong metal-support interaction (SMSI) was reported to suppress the capacity of group 8 noble metals to adsorb hydrogen and carbon monoxide by Tauster [23]. Great efforts have been made to understand the SMSI between metals and reducible supports [24,25]. The microscopic techniques play a key role in revealing the structural basis of SMSI, which was found to be the formation of an overlayer of the reducible oxide material across the metal surface [26–29]. In addition, the combination of both in situ spectroscopic and microscopic techniques (e.g., near-ambient pressure scanning tunneling microscopy) is an effective strategy to study the structure-activity relationship at a molecular level [30,31].

The detailed adsorption and activation properties of the metal catalysts fully covered by oxide overlayer are rarely reported. It is commonly thought that the oxide overlayer is apt to cover all the metal site, which renders catalysts inactive. Chen et al. constructed two kinds of $\text{TiO}_x/\text{Pt}(111)$ surfaces to simulate the SMSI state [32]. The evaluation results in CO oxidation showed that the fully covered oxide layer on Pt can increase its catalytic activity, with much lower apparent activation energy compared with that of Pt(111) surface. In situ wide spectral range, infrared reflection adsorption spectroscopy (IRAS), was used in this work to monitor the surface reaction and TiO_x model surfaces under reaction condition. A weak characteristic peak attributed to CO (2092 cm^{-1}) was detected both in the reaction gas and pure CO atmosphere (Figure 1A). Combined with inactivity of titanium oxide itself for CO oxidation, the active site was deduced to be exposed Pt atoms, which is located at the boundary of the domains of TiO_x layer. Figure 1B showed that the characteristic peaks of Ti–O vibrational modes ($1000\text{--}500\text{ cm}^{-1}$) are stable in the reaction, proving the stability of the SMSI state in this work. The above work provided an ideal encapsulation model with thin oxide overlayer on metal to study the structure-activity relationship in the fully covered SMSI state. The in situ IR showed its advantage in detecting the exposed metal atom with CO as the probe molecule.

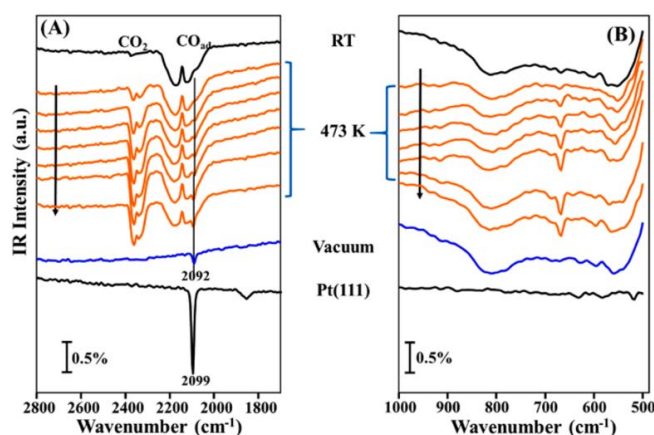


Figure 1. (A and B) In situ IRAS spectra for CO oxidation on the 1 ML (TiO_x -Re) film at 473 K. Reprinted with permission from Reference [32]. Copyright 2018, American Chemical Society.

2.2. Adsorbate-Mediated SMSI

The above work realized the enhancement of the catalytic activity of Pt catalysts by precious control of the thickness of the oxide overlayer. However, this preparation method is a high cost for the real

catalysts. Christopher et al. found an adsorbate-mediated SMSI (A-SMSI) effect, which can construct a permeable oxide overlayer for real catalysts [33]. For the Ru nanoparticles supported on TiO_2 and Nb_2O_5 , the A-SMSI encapsulation state was constructed by the treatment in $\text{CO}_2\text{-H}_2$ atmosphere at 150–300 °C. In situ IR spectroscopy (Figure 2) showed that the treatment in $20\text{CO}_2:2\text{H}_2$ atmosphere leads to the formation of formate (HCO_2 , 1531 and 1351 cm^{-1}) and a bicarbonate-like species on the TiO_2 surface (HCO_3 , 1444 cm^{-1}). At the same time, the redshift and decreased intensity of the CO characteristic peak was due to charge transfer from TiO_x to Rh and the partial physical blocking of metal sites. Combined with the previous reports of HCO_x -induced TiO_2 reduction [34–36], the A-SMSI effect was proven. Although the A-SMSI state covered the Ru nanoparticles, the oxide overlayer was permeable for reactants which provided a possible method to modulate the catalytic selectivity with acceptable activity. In this work, the in situ IR shows its advantage in detecting the adsorbed species.

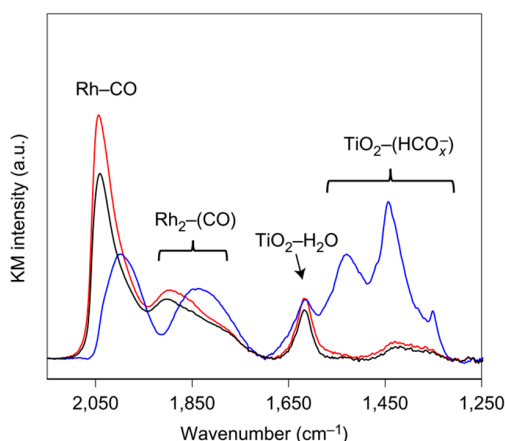


Figure 2. In situ DRIFT spectra collected from 2% Rh/ TiO_2 at the reaction conditions (180 °C, 1% CO_2 , 1% H_2 , 98 % He) for reduced (**red**), $20\text{CO}_2:2\text{H}_2$ treated (**blue**), re-reduce (**black**) catalysts. On $20\text{CO}_2:2\text{H}_2$ treatment, the CO stretching frequency of linear and bridge Rh-carbonyl groups decreased by 50 cm^{-1} , their intensity dropped twofold and TiO_2 -bound HCO_x species appeared. Re-reduction reversed all the effects of the $20\text{CO}_2:2\text{H}_2$ treatment. Reprinted with permission from Reference [33]. Copyright 2016, Springer Nature.

2.3. Wet-Chemistry SMSI Effect

The constructions of classical SMSI often rely on the redox treatments at high temperature, which probably result in sintering of the supported metal and loss of the surface area. Recently, Xiao et al. proposed the wet-chemistry SMSI (wcSMSI) effect for Au/ TiO_2 catalysts [37]. By a redox interaction between $\text{Au}^{\delta+}$ and Ti^{3+} , the Au nanoparticles can be covered by TiO_x overlayer. In situ UV-vis spectroscopy and XPS were used to study the redox interaction in this process. For the TiCl_3 solution, there was a sole peak attributed to Ti^{3+} (Figure 3A-a, 205–230 nm). When the acidity was decreased by adding a slight amount of NaHCO_3 , the bands of TiO_2 showed redshift (210–260 nm). This is due to the hydrolysis of TiCl_3 . When the Au nanoparticles were introduced into the solution, the peak intensity of Ti^{3+} increased greatly, confirming the fast formation of abundant TiO_x species (Figure 3A-f). When TiCl_3 was introduced into the Au colloid, the drastically increased band of Ti^{3+} also showed up. These results confirmed the strong redox interaction in the preparation process.

The XPS spectra (Figure 4) showed that the chemical state of Au colloids is primarily metallic Au (87.5 and 83.8 eV) and Au^+ species (88.4 and 84.7 eV). After the adding of Ti^{3+} solution, the Au species converted to negatively charge $\text{Au}^{\delta-}$ (87.1 and 83.4 eV). At the same time, the signals of Ti^{3+} diminished, indicating the transformation of Ti^{3+} to Ti^{4+} in this process. In addition, for the metal catalysts on the inert support, the methodology can also be used to tune their catalytic performance via TiO_x overlayer capsulation. In this work, the in situ spectroscopy methodology showed its wide suitability to various conditions, including the liquid environment.

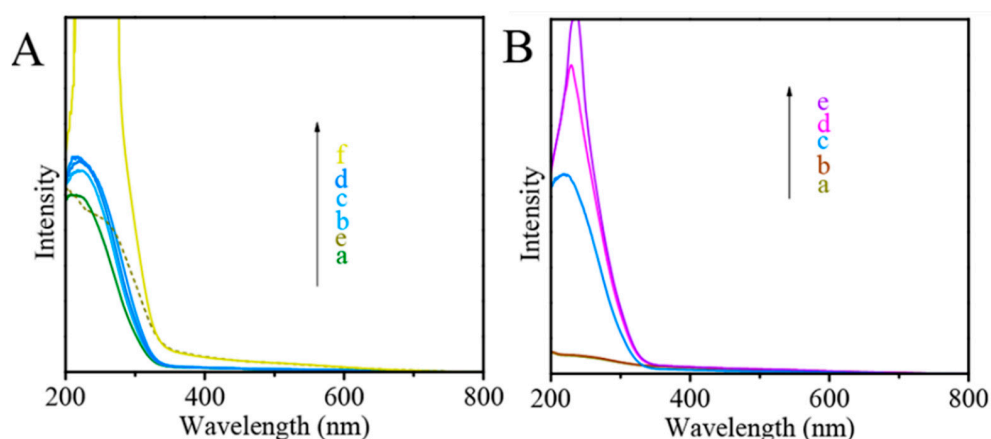


Figure 3. (A) UV-vis spectra of TiCl_3 aqueous solution (10 mg/mL) under different treatments: (a) Fresh, (b) 40, (c) 80, and (d) 200 μL of NaHCO_3 aqueous solution (4 mg/mL) was added, and (e) 750 μL of NaHCO_3 aqueous solution and 0.2 mL of Au nanoparticle colloid were added into (a), (f) 0.2 mL of Au nanoparticle colloid was added into (d); (B) UV-visible spectra of various liquors (a and b) Au nanoparticle colloid with Au concentration at (a) 0.68 and (b) 6.8 mg/L, (c–e) 40 μL of TiCl_3 aqueous solution (0.37 mg/mL) was added into (c) H_2O , (d) colloid a and (e) colloid b. Reprinted with permission from Reference [37]. Copyright 2019, American Chemical Society.

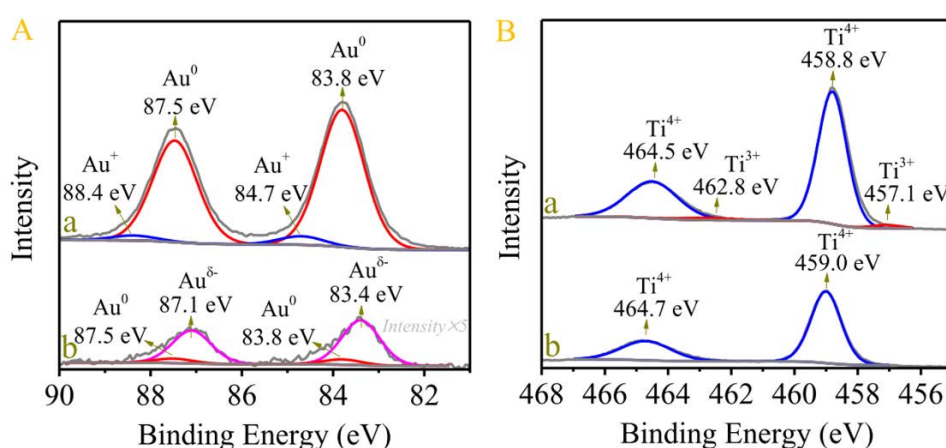


Figure 4. (A) $\text{Au}4f$ XPS spectra of Au nanoparticles (a) pretreated with O_2 and (b) interacted with Ti^{3+} ; (B) $\text{Ti}2p$ XPS spectra of the (a) as-synthesized TiO_x colloid and (b) interacting with Au nanoparticle colloid. Reprinted with permission from Reference [37]. Copyright 2019, American.

2.4. Electronic Metal-Support Interactions

In 2012, Rodriguez found a new type of strong metal-support interaction in Pt/CeO_2 catalyst, which produces large electronic perturbations for small Pt particles in contact with ceria [38]. This interaction substantially enhanced the catalytic activity of the catalyst in the dissociation of the O–H bonds in water. This type of metal-support interaction was coined as electronic metal-support interactions (EMSI) by Campbell [39]. The EMSI often leads to a special structure–activity relationship at the metal-support interfacial site, which will be discussed in the following section.

3. The Active Site at the Metal-Support Interface

In addition to the full encapsulation of metal nanoparticles with the oxide overlayer, the partially covered state results in abundant metal-support interfacial sites. At the metal-support interface, the charge transfer and support participation can greatly modulate the structures of the active sites which is significantly different from that on the metal surface. The structure-activity relationship at the

metal-support interfacial sites in catalytic reactions is summarized here, including CO oxidation, water-gas shift reaction, CO₂ hydrogenation, etc.

3.1. CO Oxidation

The best catalysts for low-temperature CO oxidation are metal catalysts supported on or promoted by reducible metal oxides, such as CeO₂ and TiO₂ [22,40,41]. There are still many open questions about this catalytic reaction system, especially the key factor in determining the reaction rate.

3.1.1. The Adsorption of CO on Au and TiO₂ at the Metal-Support Interface

The separate bulk Au and TiO₂ are inactive in CO oxidation. Compared with them, the Au/TiO₂ catalysts showed high catalytic activity in CO oxidation at low temperature. For the traditional view, the Au atoms at the metal-support interface are thought to be the active site. However, the support sites are only thought to be involved in stabilizing O₂. Yates Jr. et al. observed dual catalytic sites at the metal-support interface on Au/TiO₂ catalyst in CO oxidation [42]. The kinetic change of adsorbed CO on both Au and TiO₂ sites at the metal-support interface was monitored with in situ infrared spectroscopy (Figure 5). The CO-FTIR spectra showed the characteristic peaks of CO adsorbed on TiO₂ (2179 cm⁻¹) and Au (2102 cm⁻¹), respectively (Figure 5A). When the Au/TiO₂ catalyst with saturated CO was exposed to O₂ at 120 K, the CO adsorbed on TiO₂ disappeared gradually while CO adsorbed on Au remain almost stable (Figure 5B). In addition, almost no CO oxidation was found on pure TiO₂, indicating the key role of the metal-support interface. In response to a higher temperature, the CO adsorbed on the Au sites begin to participate in the catalytic reaction. In this work, the in situ IR showed its advantage in clearly discriminating the CO adsorbed on different sites at the metal-support interface (Au and TiO₂).

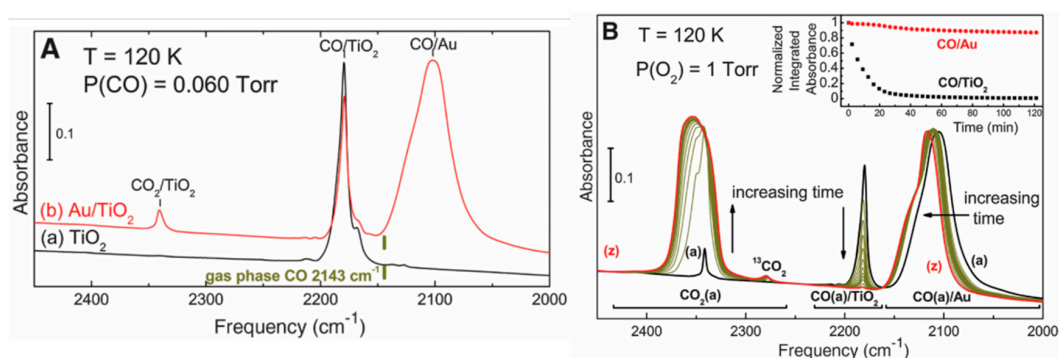


Figure 5. (A) IR spectra of saturated CO layer: Spectrum a, TiO₂; b, Au/TiO₂ under 0.060 torr of CO pressure at 120 K. (B) IR spectral development during the CO oxidation reaction on Au/TiO₂ under 1 torr of O₂ pressure at 120 K: a, before O₂ introduction; z, after 120 min of reaction. The CO/TiO₂ oxidation was found to continue when the CO coverage was replenished from spectrum z, indicating that the CO₂(a) accumulation did not block the active sites. (Inset) The plot of normalized integrated absorbance of CO/Au (red) and CO/TiO₂ (black) against time during the experiment. Reprinted with permission from Reference [42]. Copyright 2011, The American Association for the Advancement of Science.

3.1.2. The Adsorption of CO on Au Nanoparticle with Bulk Reduced TiO₂ Support

Behm et al. investigated the EMSI on bulk reduced Au/TiO₂ catalysts with in situ IR spectroscopy measurements [43]. As key evidence to prove how the EMSI affects the catalytic performance of the bulk reduced Au/TiO₂ catalyst, the in situ IR spectroscopy measurements revealed significant differences between the CO adsorption properties of metal nanoparticles supported on bulk-reduced (CO-pretreated at 400 °C, CO400) and defect-poor (O₂-pretreated at 400 °C, O400) Au/TiO₂ catalysts (Figure 6). For the CO400 catalyst exposed to the reaction gas mixture, the strong peak at 2119 cm⁻¹

is assigned to CO_{ad} on Au nanoparticles (Figure 6A). The intensity of this peak is stable for over 1000 min (Figure 6B). For the O400 catalyst, however, the peak of CO_{ad} on Au nanoparticles shows a red shift to 2116 cm^{-1} which proves that the Au nanoparticles are negatively charged. At the same time, this peak is very weak at the beginning of the reaction, showing the lower coverages of CO_{ad} . This peak gradually increases with time, together with a blue shift (from 2116 to 2119 cm^{-1}). These in situ spectroscopy studies clearly show that the EMSI on bulk-reduced Au/TiO₂ catalysts has a strong modification to the CO adsorption strength on the Au nanoparticles and likely results in lower activity in the CO oxidation reaction. In their following work, at $-20\text{ }^{\circ}\text{C}$, the in situ IR further reveals that EMSI leads to a different reaction mechanism compared with the Au-assisted Mars–van Krevelen mechanism in this work [44].

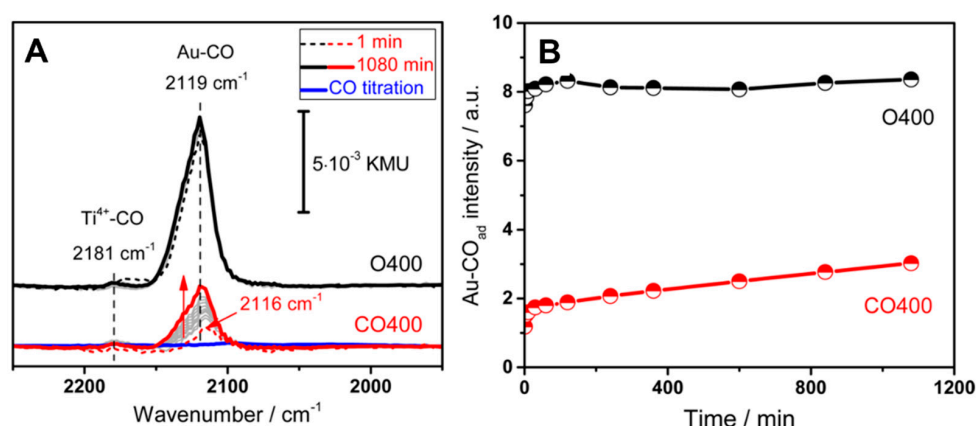


Figure 6. (A) Sequence of in situ DRIFT spectra recorded during CO oxidation (1% CO, 1% O₂, balance N₂) on Au/TiO₂ at 80 °C directly after in situ pre-treatment at 400 °C in oxidative (O400: 10% O₂/N₂) or reductive (CO400: 10% CO/N₂) atmosphere. For comparison, we also show a spectrum recorded during CO adsorption (1% CO, balance N₂, 10 min) on a CO400 catalyst. For all spectra, the gas phase CO signal is already subtracted. (B) Temporal evolution of the CO_{ad} band intensity during these measurements. Reprinted with permission from Reference [43]. Copyright 2017, American Chemical Society.

3.1.3. The Participation of Ce³⁺ Species in the Reaction at the Pt/CeO₂ Interface

For CO oxidation catalyzed by CeO₂-based metal catalysts (Pt, Pd, and Ni), kinetic studies proved that the reaction rate of CO oxidation depends on the length of the metal-support interface, rather than the nature of the metal [38]. However, the active sites and the rate-determining steps are still unclear at the molecular level. Safonova et al. applied time-resolved resonant X-ray emission spectroscopy (RXES) to quantitatively monitor the kinetics of formation and consumption of Ce³⁺ species of Pt/CeO₂ catalyst in the working conditions [45]. Figure 7 (B–E) shows the Ce³⁺ concentration measured by RXES in the atmosphere from mixed reaction gas to CO at different reaction temperatures. The initial rate of Ce³⁺ oxidation is very fast, which indicates the high activity of Ce³⁺. In addition, the Ce³⁺ does not completely disappear, proving the presence of Ce³⁺ spectator species uninvolved in the reaction. When the oxygen supply is switched off at 60 s, the concentration of Ce³⁺ increases immediately, proving the participation of oxygen from the support in the catalytic process. In this work, the relationship between the concentration of Ce³⁺ and the switched gas atmosphere clearly proved the high activity of partial Ce³⁺ in the reaction.

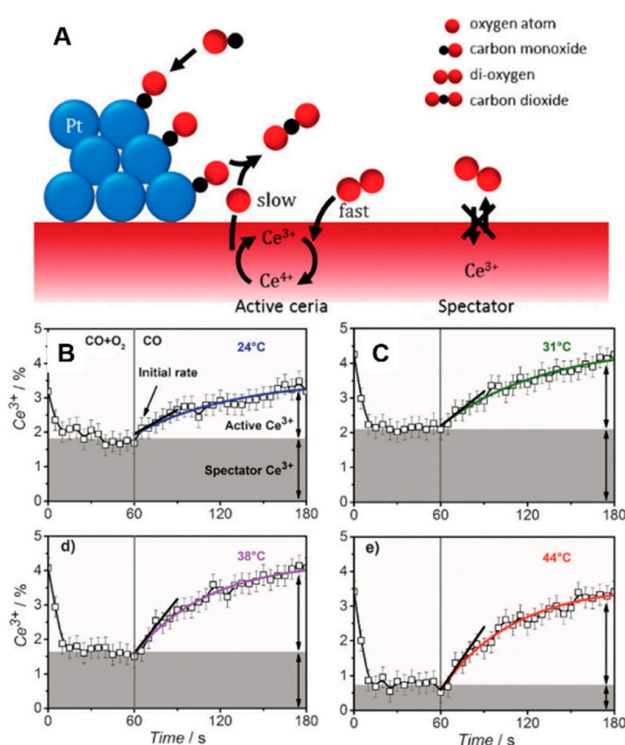


Figure 7. (A) Representation of oxygen uptake and release by ceria during the CO oxidation cycle on a Pt/CeO₂ catalyst. In the slow part of the cycle, an oxygen atom from ceria at the Pt–CeO₂ interface reacts with CO adsorbed on platinum to afford CO₂, an oxygen vacancy, and two Ce³⁺ species. The fast part of the cycle involves CO re-adsorption on platinum and oxygen activation on ceria resulting in healing of the oxygen vacancy and oxidation of active Ce³⁺ species. Ce³⁺ spectator species do not participate in CO oxidation. (B–E) Transient Ce³⁺ concentrations in the Pt/CeO₂ catalyst measured with XES during cycling between 1% CO+4% O₂ (0–60 s) and 1% CO (60–180 s) gas mixtures at 24, 31, 38, and 44 °C. The increase in Ce³⁺ concentration in 1% CO was fitted by an exponent function and the initial rate at the moment of switching (60 s) was determined (indicated as the slope). The concentrations of active and spectator Ce³⁺ species are indicated by arrows. Reprinted with permission from Reference [45]. Copyright 2015, John Wiley and Sons.

3.1.4. The Adsorbate-Driven Metal-Metal Oxide Interface Formation on the Surface of Bimetal Catalysts

In addition to the prepared metal-reducible metal oxide catalysts, Park et al. found that the interfacial Metal-Metal oxide nanostructures (Pt–NiO) are formed under a reaction condition (CO oxidation reaction) in bimetal (Pt₃Ni(111)) alloy surface, which are highly active in the CO oxidation reaction [46]. A similar interfacial nanostructure (Pt/CoO) was also found on PtCo bimetallic nanoparticles during H₂ oxidation reaction [47]. The combined in situ microscopic and spectroscopic techniques in these works helped to prove the formation of interfacial Metal-Metal oxide nanostructure.

3.2. Methane Oxidation

The reducible oxide supports play an important role in both total methane oxidation (TMO) and catalytic partial oxidation of methane (CPOM). Osman et al. found that TiO₂ support improves oxygen transport to Pd while the acidic support (H-ZSM-5) activates the methane and modifies the electrophilicity of Pd in the TMO reaction, resulting in the high activity at very low temperature (200 °C) [48]. For the CPOM catalyzed by Ni/CeO₂–ZrO₂/ZSM-5, the interfacial area between Ni and reducible metal oxides are highly active and stable. The reducible metal oxides can improve the redox cycle of Ni and supply oxygen to remove the deposited carbon [49]. The in situ/operando spectroscopic technique is relatively rarely used in this research field. In 2014, Fouladvand et al. employed the transient in situ infrared spectroscopy method to study the reaction intermediates in methane oxidation

over supported Pt catalysts [50]. The platinum-ceria interface is thought to be the additional active site resulting in the generally higher catalytic activity. In 2018, a combination of STEM-EDX and XPS analyses showed that the most active catalyst structure for combustion catalyst is dominated by alumina, with Ti found around the edges. The bimetallic Pd-Pt metals are similar to each other, dispersed across the support structure with a fairly random distribution. Thus, this work gives more information on the catalytic structure of a combustion catalyst [51].

3.3. Water–Gas Shift Reaction (WGSR)

The WGSR is an important reaction used for hydrogen production and removing CO in feed streams of fuel cells. The supports significantly affect the catalytic performance in this reaction. Osman et al. found that using acidic supports led to different interaction and synergetic effect between the two most active phases of Pt metal and Mo₂C, thus the acidity played a crucial role herein [52]. Metal nanoparticles supported on reducible metal oxides show great catalytic performance in this field. Both experimental and computational studies proved that the synergistic effect of metals and oxygen vacancies in the supports can promote the reactivity of the catalysts [13,53].

3.3.1. The EMSI at Ni^{δ-}–O_v–Ti³⁺ Interfacial Site

We have reported a TiO_{2-x}-modified Ni nanocatalyst (Ni@TiO_{2-x}) with tunable EMSI for WGS reaction [54]. In situ EXAFS verified that the increased electron density of Ni (Ni^{δ-}) results from the gradually increased reduction temperature (Figure 8). The adsorption edges of the normalized Ni K-edge XANES spectra display a gradual shift toward low photon energy with the increasing reduction temperature compared with the Ni foil, indicating the enhanced EMSI (Figure 8A). In the same process, the metallic Ni–Ni distance decreased gradually with a peak shift in Figure 8B. In addition, Figure 3C,D show that the A2 prepeaks (at ~4970.5 eV) increase and shift to lower energy, proving the existence of five-coordinated Ti atoms. The above results proved the presence of EMSI and the resulting Ni^{δ-}–O_v–Ti³⁺ interfacial site.

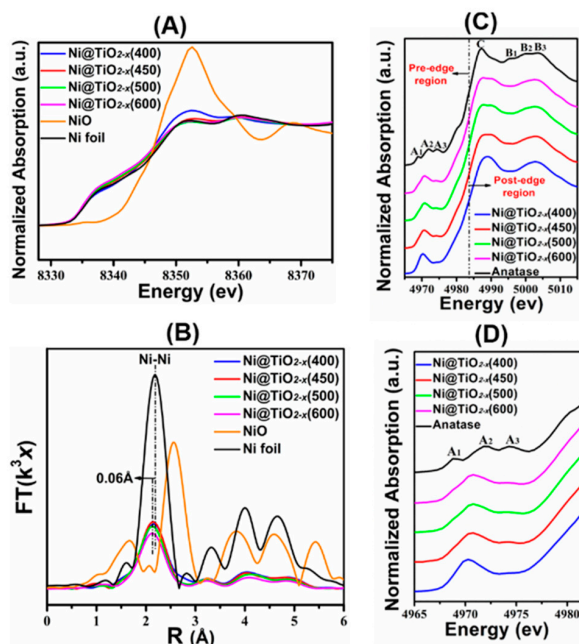


Figure 8. (A) Normalized XANES spectra at Ni K-edge for Ni@TiO_{2-x}(400), Ni@TiO_{2-x}(450), Ni@TiO_{2-x}(500), and Ni@TiO_{2-x}(600), respectively. (B) Fourier-transform EXAFS spectra at Ni K-edge for NiO reference, Ni@TiO_{2-x}(400), Ni@TiO_{2-x}(450), Ni@TiO_{2-x}(500), Ni@TiO_{2-x}(600), and Ni foil, respectively. (C) Normalized XANES spectra at Ti K-edge for Ni@TiO_{2-x}(400), Ni@TiO_{2-x}(450), Ni@TiO_{2-x}(500), and Ni@TiO_{2-x}(600), respectively. (D) The enlarged view of the absorption edge selected from (C). Reprinted with permission from Reference [54]. Copyright 2017, American Chemical Society.

3.3.2. H₂O Dissociation at Ni/TiO₂ Interface

In the above work, the quantitative relation between interfacial site and reaction rate proved that the Ni^{δ-}-O_v-Ti³⁺ interfacial site is the active site. Furthermore, the reaction mechanism of H₂O dissociation at Ni^{δ-}-O_v-Ti³⁺ interfacial site was proven by in situ EXAFS under H₂O atmosphere (Figure 9) [55]. Upon exposure to H₂O from 150 to 450 °C, the white line of Ni K-edge shifts gradually to high photon energy (Figure 9A). This indicates the oxidation of metallic Ni at elevated temperature in H₂O atmosphere. In addition, based on the FT *k*²-weighted Ni K-edge EXAFS spectra, a peak at ~3.08 Å formed at 450 °C. It is due to the formation of the Ni-O-Ti bond. In situ CO-DRIFTS measurements was also used in this work to explore the electronic structure of Ni atom at the metal-support interfacial site. These results show the efficiency of in situ spectroscopy methodology in monitoring the structural and electronic dynamic evolution of metal-support interfacial sites. Recently, EMSI was also proven to exist in Au@TiO_{2-x} catalysts [56]. In situ EXAFS proves that the metal support interfacial site is the active site for WGS. Both Au^{δ-} species and O_v directly participate in the water dissociation step (the rate-determining step for LT-WGS).

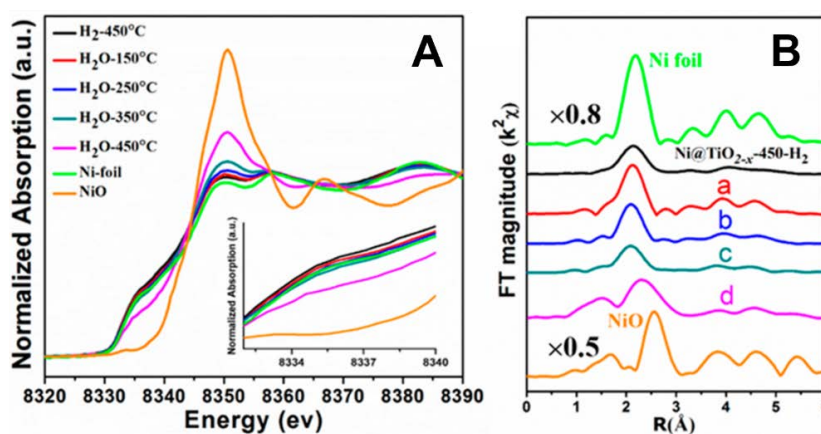


Figure 9. (A) Normalized Ni K-edge XANES spectra and (B) Fourier-transform Ni K-edge EXAFS spectra for Ni@TiO_{2-x}(450) catalyst in H₂O atmosphere at 150, 250, 350, and 450 °C, respectively. Ni foil and NiO reference sample: Room temperature. Reprinted with permission from Reference [55]. Copyright 2017, American Chemical Society.

3.4. CO₂ Hydrogenation

CO₂ hydrogenation is a promising reaction route to achieve carbon recycling. This not only contributes to the alleviation of environmental problems, but also has the potential to produce useful chemicals (e.g., CH₃OH, CO, and CH₄) [57]. Metal catalysts based on reducible metal oxides (e.g., CeO₂, TiO₂) are appropriate catalysts for CO₂ conversion. Recently, the unique structural features and key reaction intermediates at the metal-support interface have been well studied with in situ/operando spectroscopy methodology.

3.4.1. The CO₂ Hydrogenation to CH₃OH at Cu/CeO₂ Interface

Rodriguez et al. found that the catalytic rate of the CO₂ hydrogenation to methanol on CeO_x/Cu(111) is significantly faster than those on Cu(111) and Cu/ZnO(0001) [58]. The in situ infrared reflection absorption spectroscopy (IRRAS) and ambient-pressure (AP) XPS were employed to investigate the reaction intermediates at the Cu-Ce interfaces for methanol synthesis from CO₂. Under the reaction conditions (atmosphere: CO₂ + H₂, 500 K), the characteristic peaks of carboxylate (CO₂^{δ-}, 1295 cm⁻¹) and formate species (HCOO⁻, 1330, 1370, 1598, 2858 cm⁻¹) were detected (Figure 10). A similar result was obtained in the AP-XPS spectrum under CO₂/H₂ mixture at 473 K on CeO_x/Cu(111) surface. The main feature can be fitted with characteristic peaks of carboxylate (288.4 eV) and formate (289.2 eV), respectively. Considering the lower stability of carboxylate, it is a more active intermediate compared

with formate. In this work, in situ spectroscopy studies played a key role in discriminating the new active reaction intermediates (carboxylate). This shows that the $\text{CeO}_x/\text{Cu}(111)$ surface is a new active site for CO_2 activation. In their following catalytic system based on $\text{Au}/\text{CeO}_x/\text{TiO}_2$ catalyst, the catalytic role of CeO_x in activating CO_2 and the active surface intermediates were further confirmed by in situ AP-XPS [59].

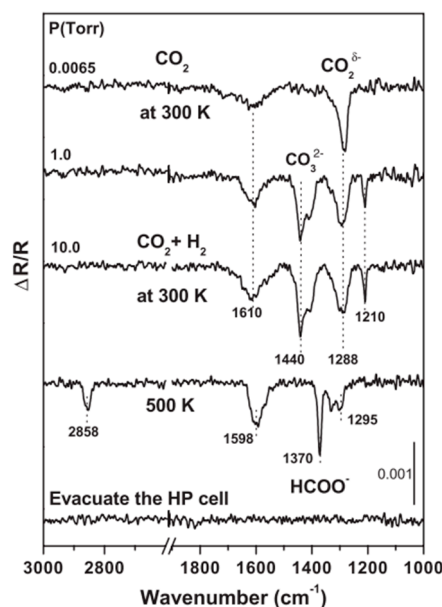


Figure 10. IRRAS spectra at ambient pressures. The spectra were obtained after the exposure of $\text{CeO}_x/\text{Cu}(111)$ to CO_2 and H_2 at the indicated pressures and temperatures. All the spectra except the one at the bottom were collected in the presence of CO_2 or a $\text{CO}_2 + \text{H}_2$ mixture at the indicated pressures. $\Delta R/R$, normalized reflectivity change. Reprinted with permission from Reference [58]. Copyright 2014, The American Association for the Advancement of Science.

3.4.2. CO_2 Hydrogenation to CO/CH_4 at PtCo/CeO_2 and PtCo/TiO_2 Interface

The metal-support interaction can introduce large electronic perturbations to the interfacial atoms. This will directly affect the bonding properties of the catalyst with different reaction intermediates at the interface. Chen et al. found that PtCo bimetallic catalysts supported on different reducible oxides (CeO_2 and TiO_2) have significantly different catalytic selectivities (CO/CH_4) in CO_2 hydrogenation reaction [60]. The in situ FTIR played a key role in illustrating this conclusion. On the one hand, formate intermediate forms on both PtCo/CeO_2 and PtCo/TiO_2 catalysts while $^*\text{CH}_3\text{O}$ only forms on PtCo/CeO_2 (Figure 11A). On the other hand, using HCOOH and CH_3OH as the probe molecules, formate and $^*\text{CH}_3\text{O}$ are likely the precursors for the formation of CO and CH_4 , respectively (Figure 11B).

3.4.3. CO_2 Hydrogenation to $\text{CH}_3\text{OH}/\text{CO}$ at the Cu/TiO_2 Interface

Chen et al. further reported the tunable selectivity in CO_2 hydrogenation over Cu/TiO_2 and Cu/ZrO_2 catalysts [61]. The in situ DRIFTS measurements played a part in detecting the adsorbate species and discriminating their relative activities. Figure 12 shows that the formation rates of $^*\text{H}_3\text{CO}$ and $^*\text{HCOO}$ are not related, indicating that the reaction does not occur via the formate route. However, the formation rate of CO is not shown by DRIFTS, which is thought to be the active reaction intermediate by the authors.

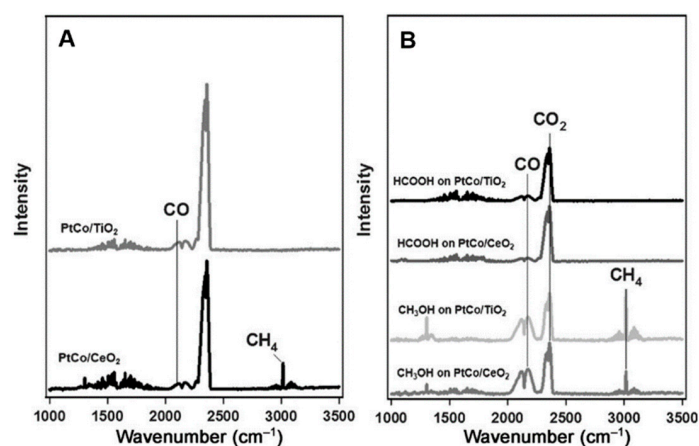


Figure 11. FTIR spectra recorded during (A) CO₂ reduction in the presence of H₂ and (B) the reactions of formic acid and methanol over PtCo/CeO₂ and PtCo/TiO₂ catalysts. Reprinted with permission from Reference [60]. Copyright 2016, John Wiley and Sons.

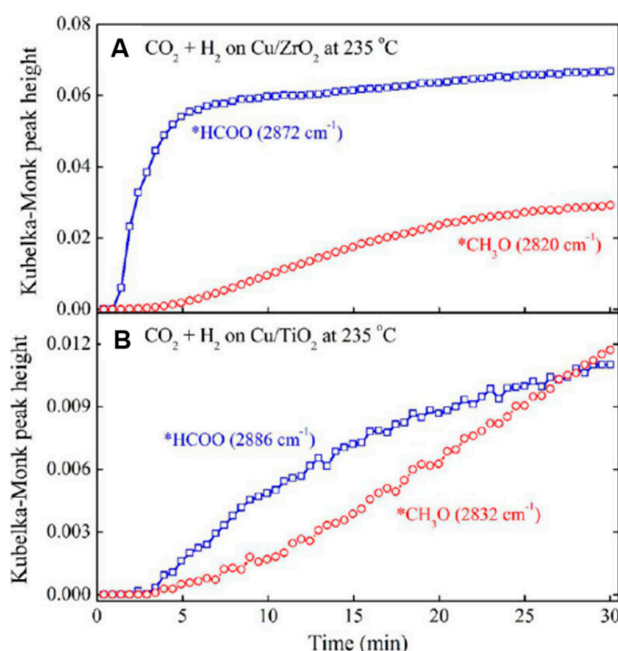


Figure 12. IR peak intensities of surface formate and methoxy species versus time during CO₂+H₂ reaction over (A) Cu/ZrO₂ and (B) Cu/TiO₂ catalysts. (Reaction conditions: 5 mL/min CO₂ + 15 mL/min H₂, 0.1 MPa, 235 °C). Reprinted with permission from Reference [61]. Copyright 2016, American Chemical Society.

3.4.4. CO₂ Hydrogenation to CH₄ at the Ru/CeO₂ Interface

The oxygen vacancy is one of the unique structures for reducible oxide, which is thought to play an important role in a variety of reactions [62]. In 2015, our work found the quantitative relation between the reaction rate and surface oxygen vacancies. This indicated that the oxygen vacancy is the active site for CO₂ methanation [63]. In order to understand the critical role of oxygen vacancies in the reaction, we used in situ XANES, IR, and Raman to study the structural evolvments of Ce³⁺, surface hydroxyl, and oxygen vacancy under the practical reaction conditions [64]. The results show that they need different activation temperature in the reaction (room temperature for Ce³⁺ and surface hydroxyl, 100 °C for oxygen vacancy). The reason is probably that they work in the different elementary steps of the catalytic cycle. The steady-state isotope transient kinetic analysis (SSITKA) type in situ DRIFT IR

proved that Ru nanoparticles serve as the active sites for the CO route starting from 250 °C (Figure 13). However, the transformation of formate to methanol and the successful production of CH₄ occur at about 100–150 °C. This is a similar temperature as that required for the activation of oxygen vacancy (about 100 to 200 °C), proving that the oxygen vacancy plays a key role in the dissociation of formate to methanol in the formate route.

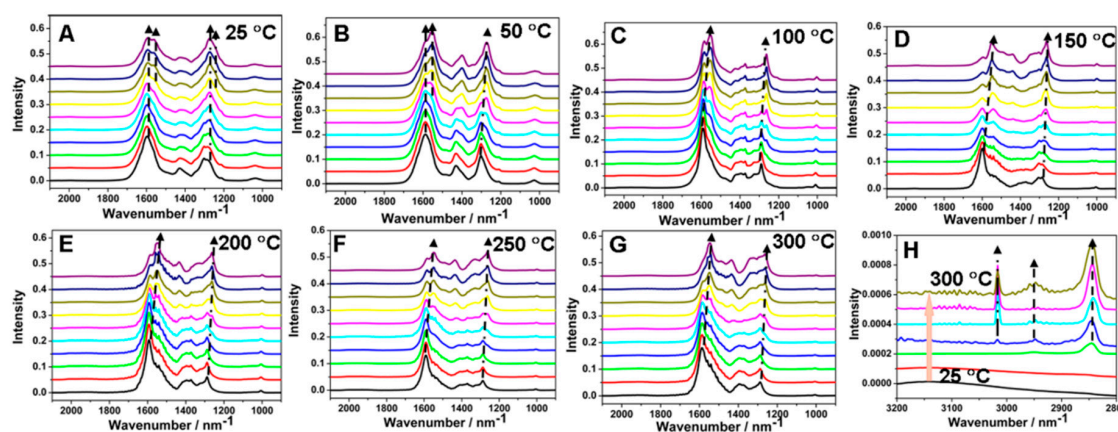


Figure 13. Operando DRIFT spectra recorded over Ru/CeO₂ catalyst by introducing 13CO₂ and H₂ as reaction gas after 90 min of equilibrium reaction in 12CO₂ and H₂. From bottom to top in each panel: 0, 0.5, 1, 1.5, 2, 3, 5, 7, 10, and 15 min. From A to G: 25, 50, 100, 150, 200, 250, and 300 °C. (H) The DRIFT spectra of CH₄ recorded over Ru/CeO₂ catalyst after 90 min of equilibrium reaction in 12CO₂ and H₂. From bottom to top: 25, 50, 100, 150, 200, 250, and 300 °C. Reprinted with permission from Reference [64]. Copyright 2016, American Chemical Society.

3.5. Unsaturated Aldehyde Hydrogenation

The ambient pressure sum frequency generation (SFG) vibrational spectroscopy is a surface sensitive method to observe surface reaction intermediates, which is commonly used on single crystals and shape-controlled nanoparticles [65]. In 2012, Somorjai et al. used SFG to probe the oxide-metal interface in the hydrogenation of furfuraldehyde for the first time [66]. The charged reaction intermediate is highly active and selective to a specific product. In 2014, a similar result was attained in the hydrogenation of crotonaldehyde on Pt/TiO₂ [67].

4. Conclusions

To add to the research on heterogeneous catalysis with reducible metal oxides as supports, this review article summarizes the recent progress using in situ/operando spectroscopy methodology. On the one hand, four kinds of intimate metal-support interactions are summarized, including the strong metal-support interaction (SMSI), adsorbate-mediated SMSI (A-SMSI), wet-chemistry SMSI (wcSMSI), and electronic metal-support interactions (EMSI). On the other hand, the structure-activity relationship at the metal-support interfacial sites in three important catalytic reactions is summarized, including CO oxidation, WGS, and CO₂ hydrogenation. Although much progress has been made, great challenges still remain in this area, some of which are listed as follows: (1) It is hard to control the extent of partial decoration of metal nanoparticles by oxide overlayers for real catalysts. The preparation of catalysts via the structure topotactic transformation of layered double hydroxide (LDHs) precursor is a good method. The reduction treatment at different temperatures can finely tune the extent of partial decoration. (2) It is a challenge to clearly make a distinction between active reaction intermediates and precursors for the adsorbed species. The steady-state isotope transient kinetic analysis (SSITKA) type in situ infrared spectroscopy is an effective method by correlating buildup/decay of surface species. However, it should be noted that the peak shift of adsorbed species may result from thermal desorption rather than catalytic conversion. (3) It is hard to confirm the real rate-determining step in

the reaction mechanism. This problem is likely due to the excessive reaction temperature, which leads to an undetectable concentration of reaction intermediate on the surface of the catalyst. The detection effect can be improved by lowering the reaction temperature. With the rapid advance of in situ/operando spectroscopy methodology, the structure-activity relationship for metal catalysts supported on reducible oxides will gradually have more light spread upon it, which will be beneficial for the rational design of heterogeneous catalysts.

Funding: This research received no external funding.

Conflicts of Interest: The authors declare no conflict of interest.

References

1. Ryczkowski, J. IR spectroscopy in catalysis. *Catal. Today* **2001**, *68*, 263–381. [[CrossRef](#)]
2. Venezia, A.M. X-ray photoelectron spectroscopy (XPS) for catalysts characterization. *Catal. Today* **2003**, *77*, 359–370. [[CrossRef](#)]
3. Stacchiola, D.J. Tuning the properties of copper-based catalysts based on molecular in situ studies of model systems. *Acc. Chem. Res.* **2015**, *48*, 2151–2158. [[CrossRef](#)] [[PubMed](#)]
4. Bañares, M.A. Operando methodology: Combination of in situ spectroscopy and simultaneous activity measurements under catalytic reaction conditions. *Catal. Today* **2005**, *100*, 71–77. [[CrossRef](#)]
5. Chakrabarti, A.; Ford, M.E.; Gregory, D.; Hu, R.; Keturakis, C.J.; Lwin, S.; Tang, Y.; Yang, Z.; Zhu, M.; Bañares, M.A.; et al. A decade plus of operando spectroscopy studies. *Catal. Today* **2017**, *283*, 27–53. [[CrossRef](#)]
6. Zanella, R.; Giorgio, S.; Shin, C.; Henry, C.R.; Louis, C. Characterization and reactivity in CO oxidation of gold nanoparticles supported on TiO₂ prepared by deposition-precipitation with NaOH and urea. *J. Catal.* **2004**, *222*, 357–367. [[CrossRef](#)]
7. Zhu, H.; Qin, Z.; Shan, W.; Shen, W.; Wang, J. Pd/CeO₂-TiO₂ catalyst for CO oxidation at low temperature: A TPR study with H₂ and CO as reducing agents. *J. Catal.* **2004**, *225*, 267–277. [[CrossRef](#)]
8. Carrettin, S.; Concepción, P.; Corma, A.; López Nieto, J.M.; Puentes, V.F. Nanocrystalline CeO₂ increases the activity of Au for CO oxidation by two orders of magnitude. *Angew. Chem. Int. Ed.* **2004**, *43*, 2538–2540. [[CrossRef](#)]
9. Wu, Z.; Li, M.; Overbury, S.H. On the structure dependence of CO oxidation over CeO₂ nanocrystals with well-defined surface planes. *J. Catal.* **2012**, *285*, 61–73. [[CrossRef](#)]
10. Luengnaruemitchai, A.; Osuwan, S.; Gulari, E. Comparative studies of low-temperature water-gas shift reaction over Pt/CeO₂, Au/CeO₂, and Au/Fe₂O₃ catalysts. *Catal. Commun.* **2003**, *4*, 215–221. [[CrossRef](#)]
11. Fu, Q.; Weber, A.; Flytzani-Stephanopoulos, M. Nanostructured Au-CeO₂ catalysts for low-temperature water-gas shift. *Catal. Lett.* **2001**, *77*, 87–95. [[CrossRef](#)]
12. Panagiotopoulou, P.; Kondarides, D.I. Effect of morphological characteristics of TiO₂-supported noble metal catalysts on their activity for the water-gas shift reaction. *J. Catal.* **2004**, *225*, 327–336. [[CrossRef](#)]
13. Rodriguez, J.A.; Liu, P.; Hrbek, J.; Evans, J.; Pérez, M. Water gas shift reaction on Cu and Au nanoparticles supported on CeO₂(111) and ZnO(0001): Intrinsic activity and importance of support interactions. *Angew. Chem. Int. Ed.* **2007**, *46*, 1329–1332. [[CrossRef](#)] [[PubMed](#)]
14. Park, J.N.; McFarland, E.W. A highly dispersed Pd-Mg/SiO₂ catalyst active for methanation of CO₂. *J. Catal.* **2009**, *266*, 92–97. [[CrossRef](#)]
15. Corma, A.; Garcia, H. Photocatalytic reduction of CO₂ for fuel production: Possibilities and challenges. *J. Catal.* **2013**, *308*, 168–175. [[CrossRef](#)]
16. Hakim, S.H.; Sener, C.; Alba-Rubio, A.C.; Gostanian, T.M.; O'Neill, B.J.; Ribeiro, F.H.; Miller, J.T.; Dumesic, J.A. Synthesis of supported bimetallic nanoparticles with controlled size and composition distributions for active site elucidation. *J. Catal.* **2015**, *328*, 75–90. [[CrossRef](#)]
17. Centi, G.; Iaquaniello, G.; Perathoner, S. Can we afford to waste carbon dioxide? Carbon dioxide as a valuable source of carbon for the production of light olefins. *ChemSusChem* **2011**, *4*, 1265–1273. [[CrossRef](#)]
18. Ma, J.; Sun, N.N.; Zhang, X.L.; Zhao, N.; Mao, F.K.; Wei, W.; Sun, Y.H. A short review of catalysis for CO₂ conversion. *Catal. Today* **2009**, *148*, 221–231. [[CrossRef](#)]
19. Haller, G.L.; Resasco, D.E. Metal support interaction-group—VIII metals and reducible oxides. *Adv. Catal.* **1989**, *36*, 173–235. [[CrossRef](#)]

20. Ioannides, T.; Verykios, X.E. Charge transfer in metal catalysts supported on doped TiO₂: A theoretical approach based on metal-semiconductor contact theory. *J. Catal.* **1996**, *161*, 560–569. [[CrossRef](#)]
21. Farmer, J.A.; Campbell, C.T. Ceria maintains smaller metal catalyst particles by strong metal-support bonding. *Science* **2010**, *329*, 933–936. [[CrossRef](#)]
22. Saavedra, J.; Doan, H.A.; Pursell, C.J.; Grabow, L.C.; Chandler, B.D. The critical role of water at the gold-titania interface in catalytic CO oxidation. *Science* **2014**, *345*, 1599–1602. [[CrossRef](#)]
23. Tauster, S.J.; Fung, S.C.; Garten, R.L. Strong metal-support interactions. Group VIII noble metals supported on Titania. *J. Am. Chem. Soc.* **1978**, *100*, 170–175. [[CrossRef](#)]
24. Datye, A.K.; Kalakkad, D.S.; Yao, M.H.; Smith, D.J. Comparison of metal-support interactions in Pt/TiO₂ and Pt/CeO₂. *J. Catal.* **1995**, *155*, 148–153. [[CrossRef](#)]
25. Freund, H.J.; Pacchioni, G. Oxide ultra-thin films on metals: New materials for the design of supported metal catalysts. *Chem. Soc. Rev.* **2008**, *37*, 2224–2242. [[CrossRef](#)]
26. Suzuki, T.; Souda, R. The encapsulation of Pd by the supporting TiO₂(110) surface induced by strong metal-support interactions. *Surf. Sci.* **2000**, *448*, 33–39. [[CrossRef](#)]
27. Bowker, M.; Stone, P.; Morrall, P.; Smith, R.; Bennett, R.; Perkins, N.; Kvon, R.; Pang, C.; Fourre, E.; Hall, M. Model catalyst studies of the strong metal–support interaction: Surface structure identified by STM on Pd nanoparticles on TiO₂(110). *J. Catal.* **2005**, *234*, 172–181. [[CrossRef](#)]
28. Bennett, R.A.; Pang, C.L.; Perkins, N.; Smith, R.D.; Morrall, P.; Kvon, R.I.; Bowker, M. Surface structures in the SMSI state; Pd on (1 × 2) reconstructed TiO₂(110). *J. Phys. Chem. B* **2002**, *106*, 4688–4696. [[CrossRef](#)]
29. Fu, Q.; Wagner, T.; Olliges, S.; Carstanjen, H.-Z. Metal-oxide interfacial reactions: Encapsulation of Pd on TiO₂(110). *J. Phys. Chem. B* **2005**, *109*, 944–951. [[CrossRef](#)]
30. Somorjai, G.A.; Park, J.Y. Frontiers of surface science. *Phys. Today* **2007**, *60*, 48–53. [[CrossRef](#)]
31. Somorjai, G.A.; York, R.L.; Butcher, D.; Park, J.Y. The evolution of model catalytic systems; studies of structure, bonding and dynamics from single crystal metal surfaces to nanoparticles, and from low pressure (<10 - 3 Torr) to high pressure (>10 - 3 Torr) to liquid interfaces. *Phys. Chem. Chem. Phys.* **2007**, *9*, 3500–3513. [[CrossRef](#)]
32. Li, H.; Weng, X.; Tang, Z.; Zhang, H.; Ding, D.; Chen, M.; Wan, H. Evidence of the encapsulation model for strong metal-support interaction under oxidized conditions: A case study on TiO_x/Pt(111) for CO oxidation by in situ wide spectral range infrared reflection adsorption spectroscopy. *ACS Catal.* **2018**, *8*, 10156–10163. [[CrossRef](#)]
33. Matsubu, J.C.; Zhang, S.; DeRita, L.; Marinkovic, N.S.; Chen, J.G.; Graham, G.W.; Pan, X.; Christopher, P. Adsorbate-mediated strong metal-support interactions in oxide-supported Rh catalysts. *Nat. Chem.* **2017**, *9*, 120–127. [[CrossRef](#)] [[PubMed](#)]
34. Henderson, M.A. Complexity in the decomposition of formic acid on the TiO₂(110) surface. *J. Phys. Chem. B* **1997**, *101*, 221–229. [[CrossRef](#)]
35. Diebold, U. The surface science of titanium dioxide. *Surf. Sci. Rep.* **2003**, *48*, 53–229. [[CrossRef](#)]
36. Morikawa, Y.; Takahashi, I.; Aizawa, M.; Namai, Y.; Sasaki, T.; Iwasawa, Y. First-principles theoretical study and scanning tunneling microscopic observation of dehydration process of formic acid on a TiO₂(110) surface. *J. Phys. Chem. B* **2004**, *108*, 14446–14451. [[CrossRef](#)]
37. Zhang, J.; Wang, H.; Wang, L.; Ali, S.; Wang, C.; Wang, L.; Meng, X.; Li, B.; Su, D.S.; Xiao, F. Wet-chemistry strong metal-support interactions in titania supported Au catalysts. *J. Am. Chem. Soc.* **2019**, *141*, 2975–2983. [[CrossRef](#)]
38. Bruix, A.; Rodriguez, J.A.; Ramirez, P.J.; Senanayake, S.D.; Evans, J.; Park, J.B.; Stacchiola, D.; Liu, P.; Hrbek, J.; Illas, F. A new type of strong metal-support interaction and the production of H₂ through the transformation of water on Pt/CeO₂(111) and Pt/CeO_x/TiO₂(110) Catalysts. *J. Am. Chem. Soc.* **2012**, *134*, 8968–8974. [[CrossRef](#)]
39. Campbell, C.T. Catalyst-support interactions electronic perturbations. *Nat. Chem.* **2012**, *4*, 597–598. [[CrossRef](#)]
40. Cargnello, M.; Doan-Nguyen, V.T.; Gordon, T.R.; Diaz, R.E.; Stach, E.A.; Gorte, R.J.; Fornasiero, P.; Murray, C.B. Control of metal nanocrystal size reveals metal-support interface role for ceria catalysts. *Science* **2013**, *341*, 771–773. [[CrossRef](#)] [[PubMed](#)]
41. An, K.; Alayoglu, S.; Musselwhite, N.; Plamthottam, S.; Melaet, G.; Lindeman, A.E.; Somorjai, G.A. Enhanced CO oxidation rates at the interface of mesoporous oxides and Pt nanoparticles. *J. Am. Chem. Soc.* **2013**, *135*, 16689–16696. [[CrossRef](#)] [[PubMed](#)]
42. Green, I.X.; Tang, W.; Neurock, M.; Yates, J.T., Jr. Spectroscopic observation of dual catalytic sites during oxidation of CO on a Au/TiO₂ Catalyst. *Science* **2011**, *333*, 736–739. [[CrossRef](#)] [[PubMed](#)]

43. Wang, Y.; Widmann, D.; Behm, R.J. Influence of TiO₂ bulk defects on CO adsorption and CO oxidation on Au/TiO₂: Electronic metal-support interactions (EMSI) in supported Au catalysts. *ACS Catal.* **2017**, *7*, 2339–2345. [[CrossRef](#)]
44. Wang, Y.; Widmann, D.; Heenemann, M.; Diemant, T.; Biskupek, J.; Schlögl, R.; Behm, R.J. The role of electronic metal-support interactions and its temperature dependence: CO adsorption and CO oxidation on Au/TiO₂ catalysts in the presence of TiO₂ bulk defects. *J. Catal.* **2017**, *354*, 46–60. [[CrossRef](#)]
45. Kopelent, R.; van Bokhoven, J.A.; Szlachetko, J.; Edebeli, J.; Paun, C.; Nachtegaal, M.; Safonova, O.V. Catalytically active and spectator Ce³⁺ in ceria-supported metal catalysts. *Angew. Chem. Int. Ed.* **2015**, *54*, 8728–8731. [[CrossRef](#)] [[PubMed](#)]
46. Kim, J.; Park, W.H.; Doh, W.H.; Lee, S.W.; Noh, M.C.; Gallet, J.; Bournel, F.; Kondoh, H.; Mase, K.; Jung, Y.; et al. Adsorbate-driven reactive interfacial Pt-NiO_{1-x} nanostructure formation on the Pt₃Ni(111) alloy surface. *Sci. Adv.* **2018**, *4*, eaat3151. [[CrossRef](#)] [[PubMed](#)]
47. Lee, H.; Lim, J.; Lee, C.; Back, S.; An, K.; Shin, J.W.; Ryoo, R.; Jung, Y.; Park, J.Y. Boosting hot electron flux and catalytic activity at metal-oxide interfaces of PtCo bimetallic nanoparticles. *Nat. Commun.* **2018**, *9*, 2235. [[CrossRef](#)]
48. Osman, A.I.; Abu-Dahrieh, J.K.; Laffir, F.; Curtin, T.; Thompson, J.M.; Rooney, D.W. A bimetallic catalyst on a dual component support for low temperature total methane oxidation. *Appl. Catal. B* **2016**, *187*, 408–418. [[CrossRef](#)]
49. Osman, A.I.; Meudal, J.; Laffir, F.; Thompson, J.; Rooney, D. Enhanced catalytic activity of Ni on η-Al₂O₃ and ZSM-5 on addition of ceria zirconia for the partial oxidation of methane. *Appl. Catal. B* **2017**, *212*, 68–79. [[CrossRef](#)]
50. Fouladvand, S.; Skoglundh, M.; Carlsson, P. A transient in situ infrared spectroscopy study on methane oxidation over supported Pt catalysts. *Catal. Sci. Technol.* **2014**, *4*, 3463–3473. [[CrossRef](#)]
51. Osman, A.I.; Abu-Dahrieh, J.K.; McLaren, M.; Laffir, F.; Rooney, D.W. Characterisation of robust combustion catalyst from aluminium foil waste. *ChemistrySelect* **2018**, *3*, 1545–1550. [[CrossRef](#)]
52. Osman, A.I.; Abu-Dahrieh, J.K.; Cherkasov, N.; Fernandez-Garcia, J.; Walker, D.; Walton, R.I.; Rooney, D.W.; Rebrov, E. A highly active and synergistic Pt/Mo₂C/Al₂O₃ catalyst for water-gas shift reaction. *Mol. Catal.* **2018**, *455*, 38–47. [[CrossRef](#)]
53. Mudiyansele, K.; Senanayake, S.D.; Ferial, L.; Kundu, S.; Baber, A.E.; Graciani, J.; Vidal, A.B.; Agnoli, S.; Evans, J.; Chang, R.; et al. Importance of the metal-oxide interface in catalysis: In situ studies of the water-gas shift reaction by ambient-pressure X-ray photoelectron spectroscopy. *Angew. Chem. Int. Ed.* **2013**, *52*, 5101–5105. [[CrossRef](#)] [[PubMed](#)]
54. Xu, M.; He, S.; Chen, H.; Cui, G.; Zheng, L.; Wang, B.; Wei, M. TiO_{2-x}-modified Ni nanocatalyst with tunable metal-support interaction for water-gas shift reaction. *ACS Catal.* **2017**, *7*, 7600–7609. [[CrossRef](#)]
55. Xu, M.; Yao, S.; Rao, D.; Niu, Y.; Liu, N.; Peng, M.; Zhai, P.; Man, Y.; Zheng, L.; Wang, B.; et al. Insights into interfacial synergistic catalysis over Ni@TiO_{2-x} catalyst toward water-gas shift reaction. *J. Am. Chem. Soc.* **2018**, *140*, 11241–11252. [[CrossRef](#)] [[PubMed](#)]
56. Liu, N.; Xu, M.; Yang, Y.; Zhang, S.; Zhang, J.; Wang, W.; Zheng, L.; Hong, S.; Wei, M. Au^{δ-}-O_v-Ti³⁺ interfacial site: Catalytic active center toward low-temperature water gas shift reaction. *ACS Catal.* **2019**, *9*, 2707–2717. [[CrossRef](#)]
57. Wang, F.; Wei, M.; Evans, D.G.; Duan, X. CeO₂-based heterogeneous catalysts toward catalytic conversion of CO₂. *J. Mater. Chem. A* **2016**, *4*, 5773–5783. [[CrossRef](#)]
58. Graciani, J.; Mudiyansele, K.; Xu, F.; Baber, A.E.; Evans, J.; Senanayake, S.D.; Stacchiola, D.J.; Liu, P.; Hrbek, J.; Sanz, J.F.; et al. Highly active copper-ceria and copper-ceria-titania catalysts for methanol synthesis from CO₂. *Science* **2014**, *345*, 546–550. [[CrossRef](#)] [[PubMed](#)]
59. Yang, X.; Kattel, S.; Senanayake, S.D.; Boscoboinik, J.A.; Nie, X.; Graciani, J.; Rodriguez, J.A.; Liu, P.; Stacchiola, D.J.; Chen, J.G. Low pressure CO₂ hydrogenation to methanol over gold nanoparticles activated on a CeO_x/TiO₂ interface. *J. Am. Chem. Soc.* **2015**, *137*, 10104–10107. [[CrossRef](#)]
60. Kattel, S.; Yu, W.; Yang, X.; Yan, B.; Huang, Y.; Wan, W.; Liu, P.; Chen, J.G. CO₂ hydrogenation over oxide-supported PtCo catalysts: The role of the oxide support in determining the product selectivity. *Angew. Chem. Int. Ed.* **2016**, *55*, 7968–7973. [[CrossRef](#)]

61. Kattel, S.; Yan, B.; Yang, Y.; Chen, J.G.; Liu, P. Optimizing binding energies of key intermediates for CO₂ hydrogenation to methanol over oxide-supported copper. *J. Am. Chem. Soc.* **2016**, *138*, 12440–12450. [[CrossRef](#)] [[PubMed](#)]
62. Esch, F.; Fabris, S.; Zhou, L.; Montini, T.; Africh, C.; Fornasiero, P.; Comelli, G.; Roser, R. Electron localization determines defect formation on ceria substrates. *Science* **2005**, *309*, 752–755. [[CrossRef](#)] [[PubMed](#)]
63. Wang, F.; Li, C.; Zhang, X.; Wei, M.; Evans, D.G.; Duan, X. Catalytic behavior of supported Ru nanoparticles on the {100}, {110}, and {111} facet of CeO₂. *J. Catal.* **2015**, *329*, 177–186. [[CrossRef](#)]
64. Wang, F.; He, S.; Chen, H.; Wang, B.; Zheng, L.; Wei, M.; Evans, D.G.; Duan, X. Active site dependent reaction mechanism over Ru/CeO₂ catalyst toward CO₂ methanation. *J. Am. Chem. Soc.* **2016**, *138*, 6298–6305. [[CrossRef](#)] [[PubMed](#)]
65. Shen, Y.R. Surface properties probed by second-harmonic and sum-frequency generation. *Nature* **1989**, *337*, 519–525. [[CrossRef](#)]
66. Baker, L.R.; Kennedy, G.; Spronsen, M.V.; Hervier, A.; Cai, X.; Chen, S.; Wang, L.; Somorjai, G.A. Furfuraldehyde hydrogenation on titanium oxide-supported platinum nanoparticles studied by sum frequency generation vibrational spectroscopy: Acid-base catalysis explains the molecular origin of strong metal–support interactions. *J. Am. Chem. Soc.* **2012**, *134*, 14208–14216. [[CrossRef](#)] [[PubMed](#)]
67. Kennedy, G.; Baker, L.R.; Somorjai, G.A. Selective amplification of C=O bond hydrogenation on Pt/TiO₂: Catalytic reaction and sum-frequency generation vibrational spectroscopy studies of crotonaldehyde hydrogenation. *Angew. Chem. Int. Ed.* **2014**, *53*, 3405–3408. [[CrossRef](#)] [[PubMed](#)]



© 2019 by the authors. Licensee MDPI, Basel, Switzerland. This article is an open access article distributed under the terms and conditions of the Creative Commons Attribution (CC BY) license (<http://creativecommons.org/licenses/by/4.0/>).